

# New nearby, bright southern ultracool dwarfs<sup>\*</sup>

T.R. Kendall<sup>1</sup>†, H.R.A. Jones<sup>1</sup>, D.J. Pinfield<sup>1</sup>, R. S. Pokorny<sup>2</sup>, S. Folkes<sup>1</sup>,  
D. Weights<sup>1</sup>, J.S. Jenkins<sup>1</sup> and N. Mauron<sup>3</sup>

<sup>1</sup>Centre for Astrophysics Research, Science and Technology Research Institute, University of Hertfordshire, College Lane, Hatfield AL10 9AB, United Kingdom

<sup>2</sup>Yunnan Observatory Chinese Academy of Sciences, PO Box 110, 650011, Kunning, China

<sup>3</sup>Groupe d'Astrophysique, UMR 5024 CNRS, Case CC72, Place Bataillon, 34095 Montpellier Cedex 5, France

Accepted; Received; in original form

## ABSTRACT

We report the discovery of twenty-one hitherto unknown bright southern ultracool dwarfs with spectral types in the range M7 to L5.5, together with new observations of a further three late M dwarfs previously confirmed. Three more objects are already identified in the literature as high proper motion stars; we derive their spectral types for the first time. All objects were selected from the 2MASS All Sky and SuperCOSMOS point source databases on the basis of their optical/near-infrared colours, *J*-band magnitudes and proper motions. Low resolution ( $R \sim 1000$ ) *JH* spectroscopy with the ESO/NTT SOFI spectrograph has confirmed the ultracool nature of 24 targets, out of a total of 25 candidates observed. Spectral types are derived by direct comparison with template objects and compared to results from H<sub>2</sub>O and FeH indices. We also report the discovery of one binary, as revealed by SOFI acquisition imaging; spectra were taken for both components. The spectral types of the two components are L2 and L4 and the distance  $\sim 19$  pc. Spectroscopic distances and transverse velocities are derived for the sample. Two  $\sim L5$  objects lie only  $\sim 10$  pc distant. Such nearby objects are excellent targets for further study to derive their parallaxes and to search for fainter, later companions with AO and/or methane imaging.

**Key words:** stars: low mass, brown dwarfs – stars: late-type – stars: kinematics – stars: distances – infrared: stars – surveys

## 1 INTRODUCTION

In recent years, the search for faint dwarfs in the Solar neighbourhood has been the subject of much attention. Such studies have been motivated by our still highly incomplete knowledge of the Sun's coolest and least massive neighbours, as pointed out by, for example, Henry et al. (1997). M dwarfs account for around 70% of the stellar number density in the Solar neighbourhood, and yet Henry et al. (2002) estimated as many as 63% of stellar systems within 25 pc remain undiscovered, while the figure for missing systems within 10 pc may be near 25% (Reid et al. 2003), or even higher (30%; Henry et al. 2002). Current and recent searches rely primarily on proper motion (Subasavage et al. 2005; Deacon et al. 2005; Pokorny et al. 2003), in conjunction

with photometry and spectroscopic follow-up (Henry et al. 2004; Lodieu et al. 2005; Scholz, Meusinger & Jahreiss 2005; Phan-Bao & Bessell 2003; Pokorny et al. 2006).

Efforts in the field have been enormously aided by the digitization of wide-field survey plates by e.g. the SuperCOSMOS project (Hambly, Irwin & MacGillivray 2001; Henry et al. 2004), and by the advent of all-sky near-infrared surveys, most notably 2MASS (Skrutskie et al. 1997) and DENIS (Epchtein 1997), together with the Sloan Digital Sky Survey (SDSS; York et al. 2000).

Moreover, observations of the low-mass dwarf population in the Solar neighbourhood have required the establishment of two new spectral classes; the L and T dwarfs (Kirkpatrick et al. 1999; Martín et al. 1999), with effective temperatures below that of the coolest M dwarfs. These discoveries have resulted in a large part from the exploitation of all-sky surveys: we may cite Burgasser et al. (2004a) and Chiu et al. (2006) as two recent examples notable in for finding large numbers of both L and T dwarfs. In the near future, the field will be further boosted by next-generation infrared surveys, notably the UKIDSS Large Area Survey

<sup>\*</sup> Based on observations made at the European Southern Observatory, Chile (NTT/SOFI programs 076C.0382, 076D.0872 and 077C.0117) and on data from the 2MASS project (University of Massachusetts and IPAC/Caltech, USA).

† E-mail: trk@star.herts.ac.uk

(Lawrence et al. 2006). New L and T dwarf discoveries are increasingly populating the immediate Solar neighbourhood.

In this paper, we report the discovery of twenty-one new ultracool dwarfs (later than M6; Bouy et al. 2005), the majority of which are estimated spectroscopically to lie closer than  $\sim 30$  pc, and which have spectral types later than M7. The two latest objects, with  $\sim$ L4-L6 spectral types, are good candidates to be very nearby; close to 10 pc, and with reference to theoretical isochrones (Baraffe et al. 2003), are very likely substellar, i.e. with masses below the hydrogen burning limit of  $0.072 M_{\odot}$  (Leggett et al. 2001). In the next Section, we overview the aims of this research and methods of target selection. The spectroscopic observations are detailed in Sect. 3. In Sect 4., we present our results and discuss the methods we have used to analyse our spectra and derive spectroscopic distances and transverse velocities for the targets. These results are discussed in Sect. 5. In Sect. 6 we show that one of the targets is a binary, with  $\sim$ L2 and  $\sim$ L4 components. A summary of our conclusions is presented in Sect. 7.

## 2 SURVEY AIMS AND TARGET SELECTION

### 2.1 Survey overview and goals

The aim of this project is to locate the remaining undiscovered, yet apparently bright, southern ultracool dwarfs in the Solar neighbourhood. By primarily using a combination of their red optical and near-infrared colours, and secondarily *via* selecting objects from this photometric sample which have the highest reduced proper motions, the survey presented here is designed to reveal bright, and therefore nearby dwarfs undiscovered by previous studies. By requiring candidates to have an *R*-band detection, the search is biased towards nearer and/or more intrinsically bright, earlier type dwarfs. A secondary bias is introduced by the use of the reduced proper motion, which as a combination of absolute magnitude and transverse velocity (Pokorny et al. 2003) may lead to the preferential discovery of high velocity objects with possible thick-disk or halo kinematics. In general, however, our aim is to find those ultracool dwarfs, optically bright enough to be detected in the SuperCOSMOS database, which lie above our reduced proper motion threshold. This corresponds to only a few  $\times 10^2$   $\text{mas yr}^{-1}$  in most cases (see Table 1).

### 2.2 Target selection

Targets were selected by interrogation of the current photometric and kinematic data provided by the 2MASS All-Sky point source and SuperCOSMOS<sup>1</sup> surveys covering the complete Southern Hemisphere. Candidate ultracool dwarfs were drawn from 2MASS with  $|b| > 10^{\circ}$ , and with *JHK* data passing cuts based on those of Cruz et al. (2003). Preliminary cuts on the 2MASS sample were:

$$\begin{aligned} 11 &\leq J \leq 17 \\ J - K &> 1 \\ J &\leq 3 \times (J - K) + 10.5 \end{aligned}$$

<sup>1</sup> <http://surveys.roe.ac.uk/ssa/>

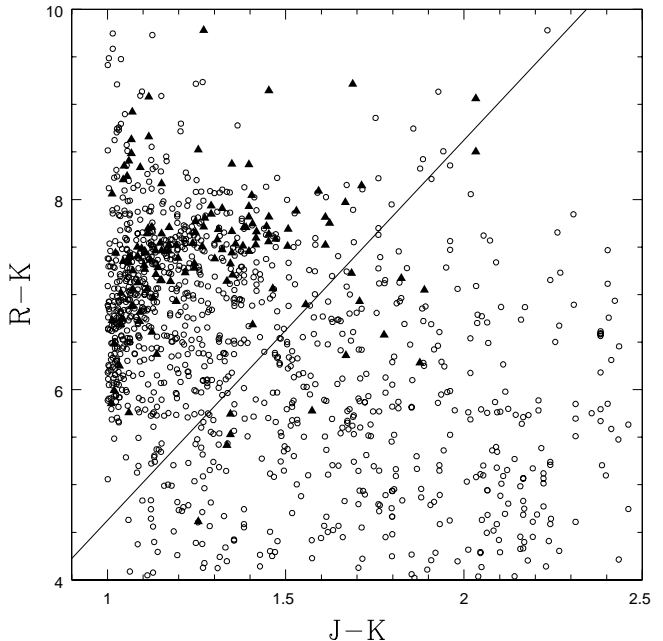


**Figure 1.** Illustration of the  $R - K, J - K$  cut used to select candidate ultracool dwarfs. Known such objects (filled triangles) lie above and to the left of the line shown. Candidates (circles) in this region were retained.

yielding an initial sample of 1055887 2MASS objects, which was immediately reduced to 109237 by removing any point with photometric quality flag 'U' (upper limit) on any magnitudes.

Excluding 52387 objects in regions of high stellar surface density (e.g. the LMC and SMC, star-forming and other regions at low galactic latitude defined by Cruz et al. (2003), with very slight modifications), the search yielded 8101 objects simultaneously satisfying the following cuts:

$$\begin{aligned} (J - H) &\leq 1.75 \times (H - K) + 0.1875 \\ (J - H) &\geq 1.75 \times (H - K) - 0.475 \end{aligned}$$

and additionally:

$$\begin{aligned} (J - H) &\leq 0.8 \text{ where } 0.3 \leq (H - K) \leq 0.35 \\ (J - H) &> 1 - (H - K) \end{aligned}$$

where the last cut is a translation of the initial  $J - K > 1$  criterion.

Objects with  $\delta \gtrsim 3^{\circ}$  were not considered further, so as to ensure SuperCOSMOS optical coverage of the sample, keeping 4074 objects, and of these only 2MASS photometry better than flag = CCC (SNR  $\geq 5$  and  $\Delta JHK \leq 0.2$ ), was kept, retaining 2317 objects.

A search radius of  $18''$  was used to search for a SuperCOSMOS optical counterpart for each object, to allow for proper motion, and which, given the typical difference in epoch between the two surveys ( $\sim 20$  yr) allowed retention of candidate field dwarfs with  $\mu_{\text{tot}}$  up to  $\sim 1'' \text{ yr}^{-1}$ . Although closer epoch differences could allow higher  $\mu$  objects through, with possibly less accurate measurements, this survey has not been designed to yield the very highest proper motion objects, which are in any case expected to be far less numerous. In contrast to, for example Pokorny et al. (2006)

Landscape Table 1 to go here.

**Table 1.**

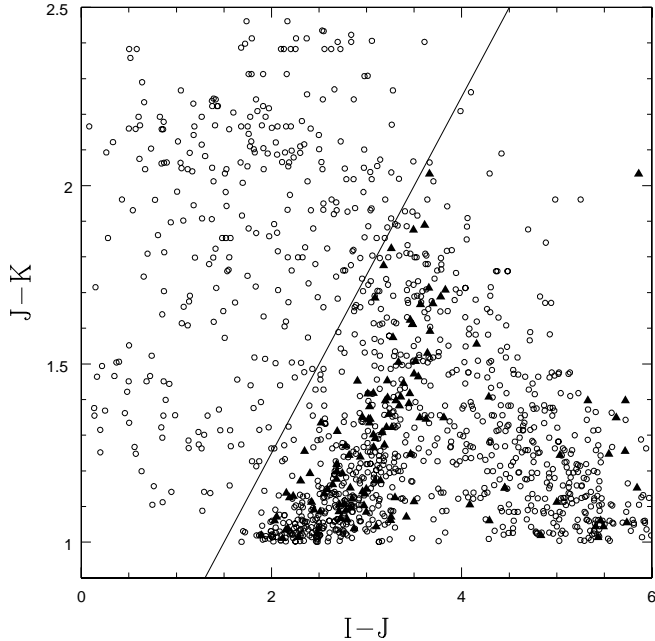


**Figure 2.** As Fig. 1, for  $J - K, I - J$ . Candidates lie below and to the right of the line shown.

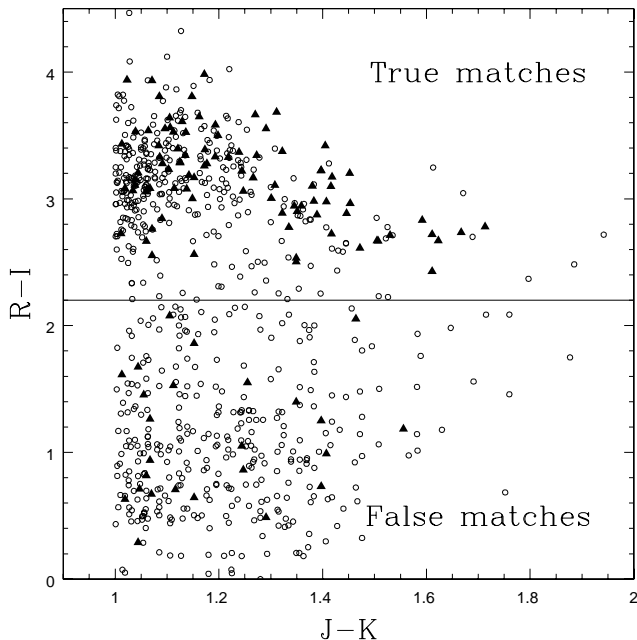


**Figure 3.** Illustration of the removal of false matches with the SuperCOSMOS  $R - I$  colour. True matches to known ultracool dwarfs lie above the horizontal line.

and Deacon et al. (2005), this research instead is primarily designed to find late-type ( $\gtrsim M7$ ), ultracool dwarfs *via* a combination of their optical and near-infrared colours, using proper motion to remove more distant contaminants.

At the same time, a total of 135 known ultracool objects taken mostly from Cruz et al. (2003) were found in

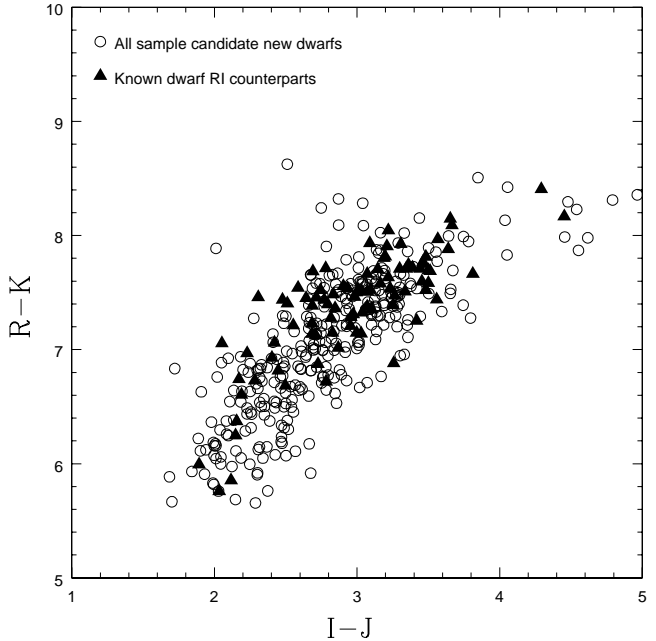


**Figure 4.** Efficiency of the  $R - K$  colour to select ultracool dwarfs. The plot shows 90 out of 103 known dwarfs with spectral types M6 or later and with SuperCOSMOS  $RI$  counterparts retained by our photometric selection methods (triangles). Circles are 317 candidates occupying the same region of the  $R - K, I - J$  diagram, from which 61 high proper motion candidates were drawn.

the SuperCOSMOS data (i.e. there was one or more optical counterpart with  $R$  and  $I$  photometry) and a total of 1245 other counterparts to the 2MASS data were also found, but these included false matches and a high proportion of contaminating objects (e.g. AGB carbon stars). Further cuts were therefore applied to the dataset of optical counterparts to the 2317 2MASS sources, to retain as many known ultracool dwarfs and discard other data points, using the loci of known objects in the  $R - K, J - K$  (Fig. 1) and  $J - K, I - J$  (Fig. 2) diagrams as a guide. These cuts were:

$$\begin{aligned} (R - K) &\geq 4 \times (J - K) + 0.625 \\ (J - K) &\leq 0.5 \times (I - J) + 0.25 \end{aligned}$$

together with:

$$5.5 \leq (R - K) \leq 9$$

to isolate L dwarfs.

Moreover, false matches were almost completely removed by rejecting points with  $(R - I) \leq 2.2$  (Fig. 3), although note that the SuperCosmos  $R$  filter does not have the same characteristics as Cousins  $R$ , so this last cut is not necessarily applicable when comparing 2MASS magnitudes to optical magnitudes from other surveys. Ninety known dwarfs were retained out of 103 passing the first three near infrared-only colour cuts. New candidate L dwarfs with optical counterparts passing the above optical/near-infrared cuts numbered 317 in total. The efficiency of the  $R - K$  colour to select ultracool dwarfs is shown in Fig. 4 where the 90 known objects and 317 potential candidate new dwarfs are shown to occupy the same region of the  $R - K, I - J$  diagram. Indeed, a 2D Kolmogorov-Smirnov test shows this is the case

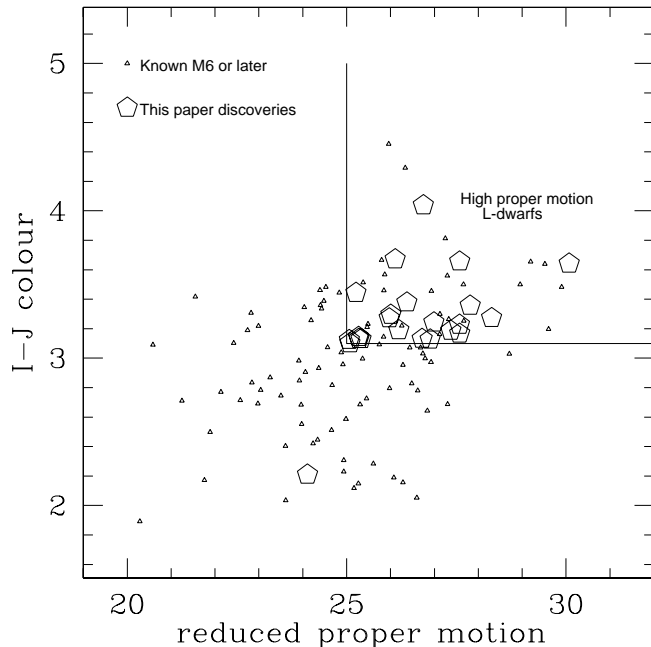


**Figure 5.** Selection of targets by reduced proper motion ( $H_J = J + 5\log(\mu_{\text{tot}})$  with  $\mu$  in  $\text{mas yr}^{-1}$ ) and  $I - J$  colour. Small triangles are data for the 90 known L dwarfs retained by our selection methods (see text) *after* use of optical vs. infrared colour criteria. The new object outside the selection criteria was originally mismatched in the 2MASS/SuperCOSMOS cross-correlation.

with 99.3% probability. Our final southern sample consists of 61 of these 317, selected to have reduced proper motion  $H_J \geq 25$  (in milliarcsecond units) and  $(I - J) \geq 3.1$ , typical for L dwarfs (Kendall et al. 2004). The 90 known L dwarfs passing these photometric cuts are plotted in Fig. 5 together with the 21 new discoveries presented here, and three further late M/early L objects from Lodieu et al. (2005) for which we present new spectroscopic data. In the last part of the selection process, candidates appearing in the SIMBAD database, or as unpublished objects listed in DwarfArchives.org<sup>2</sup>, or rejected by visual inspection of the SuperCOSMOS  $R$ -band images, were removed. 25 targets remained after this last rejection process, and 24 out of 25 targets observed spectroscopically are found here to be ultracool dwarfs later than  $\sim M7$ , the one interloper being a reddened early-type object, as evidenced by the low stellar density in the surrounding  $5' \times 5'$  SuperCOSMOS  $I$ -band field and despite the high galactic latitude  $b = -36^\circ$ . Optical and infrared photometry are given in Table 1 together with proper motions and other basic data. Derived spectral types, spectroscopic distances and transverse velocities are given in Table 2. We give details of the methods used to determine these in Sect. 4.

### 3 SPECTROSCOPIC OBSERVATIONS AND DATA REDUCTION

Observations were carried out in three runs at the ESO New Technology Telescope (NTT) with the SOFI spectrograph, during October 25–29, 2005, January 17–19, 2006 and April 4–7, 2006, allowing observation of the complete sample of southern targets at all RAs. The  $0.6''$  slit was employed with the blue  $JH$  grism yielding a wavelength coverage of 9300–16500 Å at a spectral resolution  $R = \lambda/\Delta\lambda \sim 1000$ . The detector is a Hawaii HgCdTe  $1024 \times 1024$  array with  $18.5 \mu\text{m}$  pixels. Accurate sky subtraction was facilitated by nodding the telescope along the slit, typically by  $30\text{--}45''$ . Detector integration times (DIT) were in the range 60 sec to 120 sec, with between 4 and 12 integrations at each nod position, yielding total integration times for science targets ranging between 16 and 48 min, depending on target  $J$  magnitude. The resulting spectra have signal-to-noise ratios of at least  $\sim 100$  and often better. Conditions were generally good with optical seeing in the range  $0.6''\text{--}1''$ ; however during the January 2006 run in particular, conditions of high humidity saturated the telluric  $\text{H}_2\text{O}$  band at  $1.35 \mu\text{m}$  and prevented its accurate removal. A, F or late B-type telluric standards were observed before and after each target observation at airmasses within 0.1 and often within 0.05 of the target. Dome flats and xenon lamp arcs were taken each afternoon, and again at the end of the night. Observations of template M6.5, M9, L1, L3 and L5 dwarfs were taken with the same instrumental setup; multiple observations of some of these standard stars were obtained during different observing runs.

Data reduction was undertaken within the IRAF<sup>3</sup> environment, using standard techniques for the reduction of infrared spectroscopic data. As the data covers the region between the  $J$  and  $H$ -bands, the master flatfields contain regions where structure in the dispersion direction was present (owing to the water vapour column between the dome and detector). These were interpolated using the *fixpix* routine. This means that in these regions there is no correction for pixel-to-pixel variation, but only regions of strong telluric absorption are affected. A normalised flatfield was obtained by dividing the master flat by the same image smoothed by an  $11 \times 11$  pixel boxcar. All science and telluric standard frames were divided by the normalised flat.

After flatfielding, science frames taken in each nod position were subtracted pairwise and spectra extracted using the *apall* routine. Optimal and non-optimal extractions were identical to within typically  $\lesssim$  a few %. Arc spectra were extracted using a profile of a relatively bright target star and calibrated with the *identify* and *reidentify* routines. The fit to the dispersion has typical RMS  $\sim 0.1 \text{ \AA}$ . Individual spectra were only summed (using the *sarith* routine with no pixel rejection) after wavelength calibration. Telluric correction was again performed using *sarith*; no attempts were made to scale or shift the telluric spectrum to improve the correction. Hydrogen lines at  $0.954$ ,  $1.005$ ,  $1.092$  and  $1.282 \mu\text{m}$  were removed from the telluric spectra within the *splot* routine,

<sup>3</sup> IRAF is distributed by the National Optical Astronomy Observatories, which is operated by the Association of Universities for Research in Astronomy, Inc. (AURA) under cooperative agreement with the National Science Foundation.

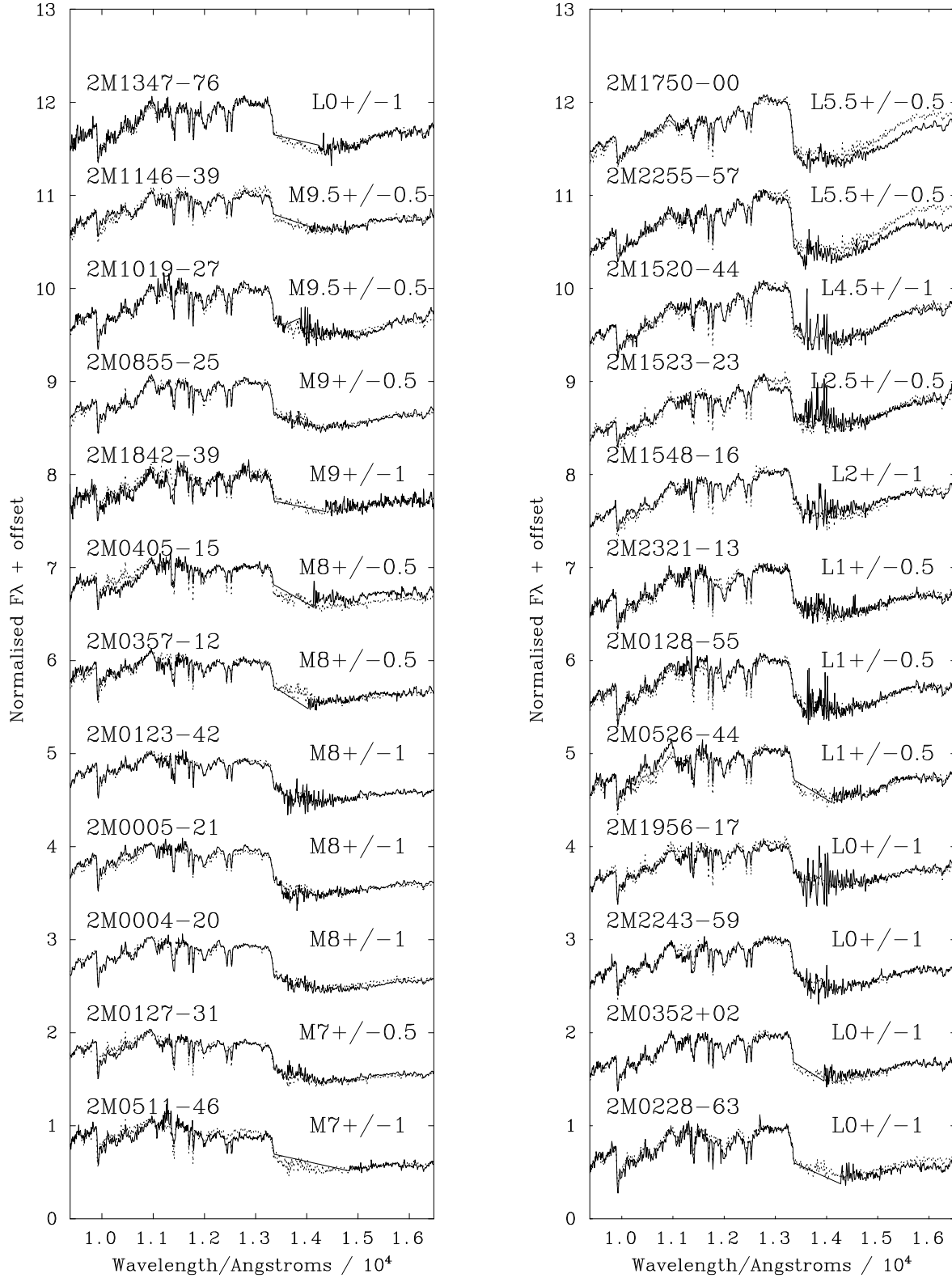


**Figure 6.** Spectral types by direct comparison to SpeX standards (Cushing et al. 2005) and known objects observed with the same instrumental setup as the targets. Unweighted means of adjacent ( $\lesssim 1$  subclass) standards from both datasets were permitted to obtain the best fits to the spectra for new objects.

**Table 2.** Derived data for the target objects. Comparison of spectral types from direct comparison (col. 5, see Fig. 6) with spectral types derived from the spectral indices of Slesnick et al. (2004) (cols. 2 & 4) and McLean et al. (2003) (col. 3; see Sect. 4.2). Where the H<sub>2</sub>O-1 index is affected by poor telluric correction, no value is given. The FeH index is invalid for spectral types later than  $\sim$ L3. Col. 6 gives the spectroscopic distance with errors reflecting the stated error on the spectral type, itself derived by comparison to template objects. Errors on transverse velocities (Col. 7) reflect only the error on the distance.

Name	H <sub>2</sub> O-1	H <sub>2</sub> O-B	FeH	spec.	d/pc	v <sub>trans</sub> /km s <sup>-1</sup>
2M0004-20	L0.5	L0	M9	M8 ± 1	17.7 <sup>+3.8</sup> <sub>-2.7</sub>	69.3 ± 12.1
2M0005-21	L0	M9.5	M9	M8 ± 1	26.5 <sup>+5.7</sup> <sub>-3.5</sub>	83.0 ± 14.4
2M0123-42	M8	M9.5	M9	M8 ± 1	25.1 <sup>+5.4</sup> <sub>-3.3</sub>	31.8 ± 5.4
2M0127-31	M9	M9	M7	M7 ± 0.5	24.3 <sup>+3.3</sup> <sub>-2.4</sub>	39.4 ± 4.5
2M0128-55	L2.5	L3	L1	L1 ± 0.5	22.7 <sup>+1.5</sup> <sub>-1.5</sub>	31.5 ± 2.1
2M0228-63	-	L1.5	L2	L0 ± 1	23.2 <sup>+3.0</sup> <sub>-2.7</sub>	70.0 ± 8.5
2M0352+02	-	L0.5	M9.5	L0 ± 1	18.6 <sup>+2.1</sup> <sub>-2.2</sub>	40.2 ± 5.0
2M0357-12	-	M9	M7.5	M8 ± 0.5	28.9 <sup>+2.7</sup> <sub>-2.1</sub>	18.5 ± 1.5
2M0405-15	-	M8.5	M8	M8 ± 0.5	30.1 <sup>+2.8</sup> <sub>-2.2</sub>	40.1 ± 3.3
2M0511-46	-	M8.5	M8	M7 ± 1	42.8 <sup>+14.0</sup> <sub>-7.5</sub>	35.1 ± 8.8
2M0526-44	-	L2	M9.5	L1 ± 0.5	26.1 <sup>+1.7</sup> <sub>-1.7</sub>	20.8 ± 1.4
2M0855-25	L0	L1	M9.5	M9 ± 0.5	22.8 <sup>+1.6</sup> <sub>-1.4</sub>	41.8 ± 2.8
2M1019-27	M9	L1	L0	M9.5 ± 0.5	24.3 <sup>+1.4</sup> <sub>-1.4</sub>	74.2 ± 4.6
2M1146-39	-	L1.5	M9	M9.5 ± 0.5	25.6 <sup>+1.6</sup> <sub>-1.5</sub>	35.4 ± 2.1
2M1347-76	-	L2	L1	L0 ± 1	25.9 <sup>+3.3</sup> <sub>-3.0</sub>	47.3 ± 5.7
2M1520-44	L3	L4	-	L4.5 ± 1	9.6 <sup>+2.2</sup> <sub>-1.9</sub>	33.7 ± 7.0
2M1523-23	L0	L2.5	L1	L2.5 ± 0.5	22.1 <sup>+1.8</sup> <sub>-1.8</sub>	36.3 ± 3.0
2M1548-16	M8.5	L1.5	L0.5	L2 ± 1	20.8 <sup>+3.2</sup> <sub>-3.2</sub>	18.6 ± 2.9
2M1750-00	L8	L6	-	L5.5 ± 0.5	8.0 <sup>+0.9</sup> <sub>-0.8</sub>	18.6 ± 1.9
2M1842-39	-	M6	M9	M9 ± 1	29.7 <sup>+4.6</sup> <sub>-3.4</sub>	88.3 ± 11.9
2M1956-17	M8	L0	M9	L0 ± 1	25.4 <sup>+3.3</sup> <sub>-3.0</sub>	21.9 ± 2.7
2M2243-59	L1	L1.5	L0	L0 ± 1	29.4 <sup>+3.8</sup> <sub>-3.4</sub>	34.0 ± 4.2
2M2255-57	L6	L7.5	-	L5.5 ± 0.5	11.5 <sup>+1.3</sup> <sub>-1.2</sub>	85.8 ± 9.0
2M2321-13	L1	L2	L3	L1 ± 0.5	31.7 <sup>+2.1</sup> <sub>-2.1</sub>	86.5 ± 5.7

before division. The telluric standard giving the best correction was normally the one closest in airmass and time but different standards from the same night were employed if they gave a better, less noisy, correction. In about 30% of the cases, part of the 1.35  $\mu$ m water band was interpolated over; in these cases there was too little flux in the region in either target or standard to provide a useful correction. Finally the spectra were multiplied by a blackbody spectrum ( $F_{\lambda}$ ) with the  $T_{\text{eff}}$  of the chosen telluric standard star, and normalised to unity at the highest point of the final spectrum.

#### 4 SPECTRAL ANALYSES

In this Section, we detail the approaches made to analyse the target spectra and derive spectral types, distances and transverse velocities. Additionally, alkali atomic line equivalent widths are measured in order to examine their behaviour with spectral type. Moreover, spectral types from  $J$ -band spectral indices are measured and compared to those derived from direct comparison with template objects.

#### 4.1 Direct comparison with templates

Our primary method of spectral typing is direct comparison of target spectra with well-observed template objects which have spectral types defined by near-infrared data. We have used the homogeneous dataset of Cushing et al. (2005) rebinned to the spectral resolution of our data, which is a factor of 2 smaller. These templates span the M and L classes down to L8. Additionally, we have used our own observations of template objects, taken with the same instrumental setup as the new objects. Best fits to the new data are shown in Fig. 6 where combinations of template spectra, with adjacent spectral types ( $\pm 1$  subclass typically) from either our data or the Cushing et al. (2005) data, or both, were created to make a best fit. The method has the advantage of using data over the whole wavelength range observed and prevents inaccuracies arising from e.g. differences in resolution between different datasets. For the remainder of this paper, we adopt these directly derived spectral types as the basis for derivation of other quantities, notably the spectroscopic distance (see Table 2). Fig. 6 shows all 24 spectra (solid line) with the best-fit template combination overplotted (dotted line). The derived spectral types and abbreviated names are indicated. It may be seen that the overall quality of the fits is excellent. Note that for the three objects already observed spectroscopically (Lodieu et al. 2005), we obtain very sim-

ilar types for two; for the third, 2M0123–42, Lodieu et al. (2005) quote L0.5, in contrast to our finding of  $M8 \pm 1$ . We do not pursue the cause of this discrepancy here, but note that in a very recent publication (Reid et al. 2006a), a spectral type of M8 is given.

## 4.2 Spectral indices

We have used indices based on the  $H_2O$ B index of McLean et al. (2003) together with the  $J$ -band FeH index of Slesnick et al. (2004) to predict spectral types for our objects. In addition we use the  $H_2O$ -I index of Slesnick et al. (2004), although this is inapplicable to  $\sim 30\%$  of our objects because of poor telluric correction, where no attempt has been made to derive the spectrum in the deepest part of the water absorption feature around  $1.35 \mu\text{m}$ . The locations and bandwidths of these indices are shown in Fig. 7 together with the main atomic and molecular features in an example mid-L object.

The results of spectral typing by this method are given in Table 2 where applicable; in those cases where poor telluric correction precludes the use of the  $H_2O$ -I index no value is given, and the FeH index is applicable only over spectral types earlier than  $\sim L3$ . Spectral types are based on the relations provided by Slesnick et al. (2004) and McLean et al. (2003) for the appropriate index.

For most objects, the spectral types derived from the indices agree well with those measured by direct comparison with templates. In some cases there appear to be small differences, for example 2M0128–55, where both water indices predict a spectral type  $\sim 2$  subclasses later. However the fit of template to observed data appears to be reasonable in this region, and in common with the other cases where indices predict types either earlier or later than the template fit (not in a systematic fashion), these differences reflect only scatter in the spectral type estimates;  $\pm 1$  subclass in general. The question of a *systematic* difference in type suggested by the indices arises only in the cases of the two latest type objects 2M1750–00 and 2M2255–57, where it is coupled with a poor fit of the template over part of the spectrum. These two cases will be discussed further later in this paper.

## 4.3 Spectroscopic distances and transverse velocities

We have derived spectroscopic distances using our infrared spectral types and the  $M_J$  vs. spectral type calibration of Cruz et al. (2003). Errors on the distances in Table 1 reflect the stated errors in spectral type propagated through the calibration. Transverse velocities have been derived using the proper motions taken from SuperCOSMOS (Table 1) and spectroscopic distances from Table 2. The results are also given in Table 2. Errors on the transverse velocities are derived using only the mean error on distance shown in Table 2; with a few exceptions, errors on the proper motions are, relatively, smaller. Although a few objects do show rather high transverse velocities, for example 2M0005–21, 2M0226–63, 2M1019–27, 2M1842–39 and 2M2255–57, no object certainly has a velocity suggestive of halo kinematics. The last object on this list, 2M2255–57, stands out because it has much the highest proper motion of this sample.

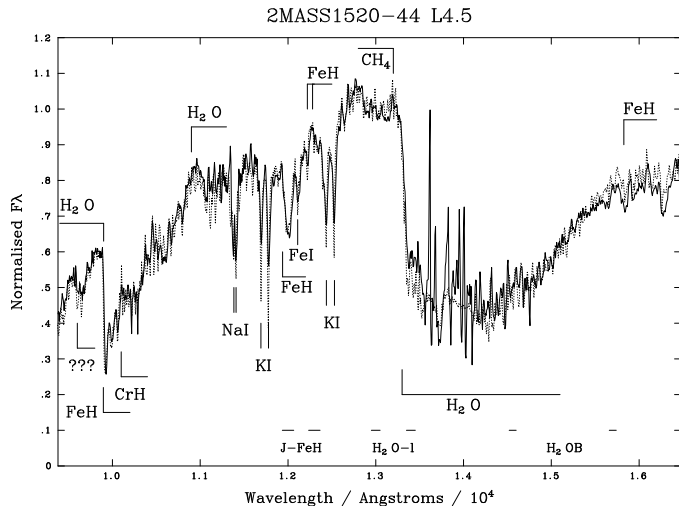


**Figure 7.** Close up of the spectrum of 2MASS1520–44, chosen for its high signal-to-noise ratio and late spectral type (L4.5). The main features present in our wavelength range are labelled together with the locations and bandwidths of the spectral indices we have used for spectral analysis. The band at  $9650 \text{ \AA}$  is not yet identified with certainty but may be FeH; see the discussion in Burgasser et al. (2003).

However, in common with three objects from Kendall et al. (2004), transverse velocities of several tens of  $\text{km s}^{-1}$  (rather than just a few tens) are observed and may be an indication that such objects do belong to a dynamically older dwarf population. Indeed, according to Burgasser (2004b), a transverse velocity of  $90 \text{ km s}^{-1}$  may indicate halo kinematics when coupled with a high radial velocity and high proper motion, as in the case of the two currently known L subdwarfs 2M0532+82 and 2M1626+39 (Burgasser et al. 2003; Burgasser 2004b). Our data are not of sufficiently high resolution to infer radial velocities, and thus intrinsic space velocities, accurately. Further study of 2M2255–57, to derive its radial velocity and therefore intrinsic space motion, is required to settle the matter. The same is true of the other objects with rather high  $v_{\text{trans}}$  listed above, although only in the case of 2M2255–57 is there any possible *spectral* evidence for an unusual nature (see Sect. 5).

## 4.4 Alkali line equivalent widths

In order to seek any objects with unusual spectral properties, for example older objects with lower metallicities and high gravities, (which could be revealed as consistent with possibly halo-type kinematics, as discussed above) we have plotted in Fig. 8 equivalent widths of the strong K I and Na I lines seen in our spectra, against spectral type. Also plotted as crosses are equivalent width data for a set of well-known ultracool dwarfs from Reid et al. (2001). Equivalent widths were measured relative to the local pseudocontinuum using the IRAF *plot* routine. Errors are  $\sim \pm 1\text{--}2 \text{ \AA}$  and larger for the Na I line which is affected by telluric correction uncertainties and clearly shows a greater scatter. However, as is clear from Burgasser et al. (2003), L subdwarfs show a rich  $J$ -band spectrum with atomic line strengths very similar to “normal” field L dwarfs although the lines are broader

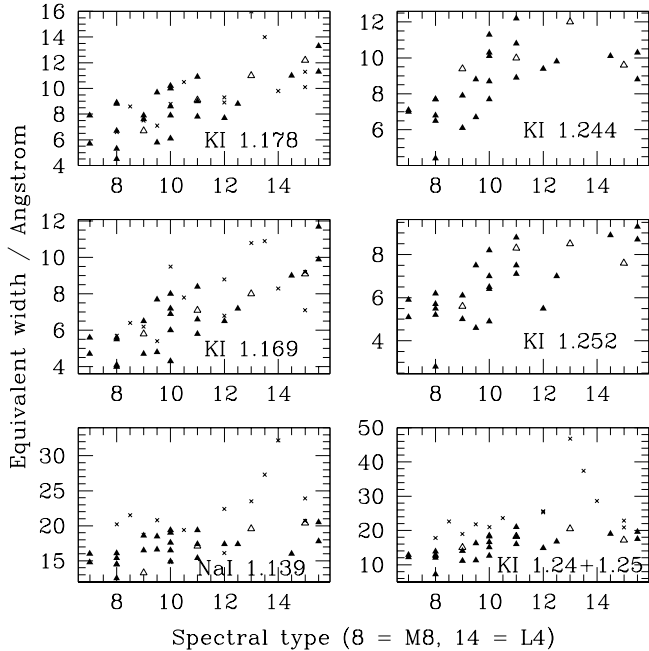


**Figure 8.** Equivalent width measurements for the 24 target objects (filled triangles) plus spectral standards observed with the same instrumental setup (open triangles) compared to equivalent width data from Reid et al. (2001) (crosses).

in the high gravity objects. Alkali lines are also strong in extreme late M subdwarfs (Burgasser & Kirkpatrick 2006). Hence atomic line strengths alone are not diagnostic of low metallicity; but also we see no evidence for unusually broad atomic lines in any of our spectra. We can though rule out the existence in our sample of young, low-gravity objects with very weak atomic lines and enhanced VO, as seen in the young field dwarf 2M J0141–46 (Kirkpatrick et al. 2006). Moreover, we observe excellent agreement between the K I 1.169 and 1.178  $\mu\text{m}$  equivalent widths of Reid et al. (2001) and our measurements. Hence, within the limitations of the data, we can conclude that none of our sample spectra appear unusual in this respect. As noted, the Na I line is affected by telluric absorption and while it appears that the equivalent widths of Reid et al. (2001) are systematically larger than our measurements, this is most likely the effect of the resulting large measurement errors. In the case of the sum of the K I 1.244 and 1.252  $\mu\text{m}$  lines in our objects, plotted in the lower right panel of Fig. 8 for comparison with Reid et al. (2001), their measurements again appear systematically larger than ours. However it is likely the Reid et al. (2001) values are measured as a blend, whereas ours are the sum of the individual line measurements. As can be seen from Figs. 6 and 7, the lines of this doublet are more blended in our spectra than those of the 1.17  $\mu\text{m}$  pair.

Thus, taking into account all these considerations, it is clear that the equivalent widths of the atomic lines in our new objects do not appear to behave differently from that predicted by their spectral type. Therefore, the analysis of alkali lines offers no evidence for the presence of low metallicity and/or high gravity (subdwarfs) or low gravity (young

objects) in the new sample of 24 ultracool dwarfs presented here.

## 5 DISCUSSION

In the analysis of *JH* band spectra of twenty four ultracool dwarfs presented above, of which twenty-one are hitherto undescribed in the literature, spectral types ranging from M7 to L5.5 are found by direct comparison to template objects taken from the homogeneous dataset of Cushing et al. (2005) together with five well described standards we have observed with the same instrumental setup. In general, we find no evidence that any of the 21 new objects have peculiar metallicities and/or kinematics. In this Section, we select individual objects from the sample for further discussion.

In particular, two L5-L6 dwarfs, 2M1750–00 and 2M2255–57, stand out in the sample, with spectroscopic distances near 10 pc. (2M1520–44, which we also place near 10 pc in Table 2, will be discussed in Sect. 6). 2M2255–57 has a large proper motion and a relatively high transverse velocity, 86  $\text{km s}^{-1}$ , while 2M1750–00 does not stand out from the sample in either respect. It is, however, apparently one of the brighter sample objects ( $J = 13.29$ ) and clearly nearby,  $\sim 8$  pc by our analysis.

For 2M1750–00 and 2M2255–57, both H<sub>2</sub>O-band indices (Table 2) predict later L spectral types, nearer L7–L8. Indeed, Fig. 6 shows that the strong H<sub>2</sub>O absorption feature is not readily fit by a combination of L5 and L6 spectral types. The reason for this is not clear. In the case of 2M2255–57, it has already been suggested that there is marginal kinematic evidence for membership of a dynamically old population. It is conceivable, then, that the apparently overly strong H<sub>2</sub>O could arise from its enhanced gravity, as is evident in the two known halo subdwarfs 2M0532+32 and 2M1626+39 (Burgasser et al. 2003; Burgasser 2004b). In this scenario, metal hydride bands would also be enhanced, leading to an under-estimation of the spectral type from the *J*-band, where the FeH bands are well fit by the L5-L6 templates. However there is no kinematic evidence for this hypothesis in the case of the other L5.5 object 2M1750–00. More importantly, for neither object is there photometric evidence of collision-induced H<sub>2</sub> absorption which would suggest a high-gravity atmosphere. This is known to result in unusually blue near-infrared colours ( $J - K \sim 0.3$ ; Burgasser 2004b) whereas both objects here have perfectly normal  $J - K$  colours,  $\sim 1.5$ . Therefore, we can probably cast doubt on the high-gravity hypothesis for both these L5.5 dwarfs, in spite of the marginal kinematic evidence for 2M2255–57.

Another possibility is that both these objects are in fact unresolved binaries, with later L-type companions with redder colours contributing relatively more to the *H*-band than the *J*-band. This would explain the fact that L5-L6 fits the *J*-band well, especially FeH. With FeH weakening towards later L types, these features in the *J*-band would be unaffected by a later companion, which could however explain the observed, deeper *H*-band H<sub>2</sub>O band, since the strength of the water absorption continues to increase throughout the later L types and into the T dwarf regime. There is no evidence for asymmetry in our acquisition images. It is clear, though, these two objects are therefore of special interest for

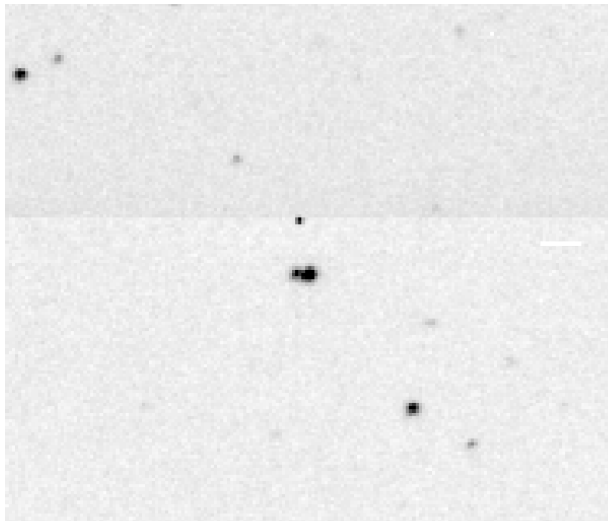


**Figure 9.** SOFI acquisition image for 2M1520–44 in the  $J$ -band. The separation is  $\sim 1''$ .

follow-up high resolution (AO or space-based) imaging in order to check for the existence of later-type companions. In this context, we note the recent discovery of the L/T binary 2MASSJ 22521073–1730134 (Reid et al. 2006b).

Finally, a general point about the whole sample; we note that although the survey is biased towards bright objects (with optical detections) it is possible that the use of the reduced proper motion may have led to a very bright, high proper motion object being missed. For example, for an object with a proper motion of  $500 \text{ mas yr}^{-1}$  to lie towards the left of the distribution of known ultracool dwarfs in Fig. 5 (for example at  $H_J = 23$ ) it would then be a bright object with  $J = 9.5$ . For an M6 dwarf ( $M_J \sim 10$ ) this corresponds to  $d \sim 8 \text{ pc}$  and for an L8 dwarf ( $M_J \sim 14.5$ ),  $d \sim 1 \text{ pc}$ . It is extremely unlikely that any such object would have been overlooked by a proper-motion only survey. However, low proper motion (low velocity) dwarfs certainly remain to be found in the remainder of the photometrically selected candidates with  $H_J < 25$  which we have not yet observed spectroscopically.

## 6 DISCOVERY OF A RESOLVED BINARY L DWARF: 2MASSJ 15200224–4422419

A spectral type of L4.5 and a spectroscopic distance near 10 pc were initially derived for 2M1520–44. However, SOFI acquisition imaging clearly resolved this object as a binary during the 2006 April 4–7 run. Therefore, supplementary spectroscopic data for 2M1520–44 were obtained on 2006 April 11 where the slit was aligned across both components. The instrumental setup was exactly as described in Sect. 3, and data reduction was performed in a similar way. The clear binary nature of this L dwarf is apparent in the acquisition image shown in Fig. 9. However, poor seeing meant that the two adjacent stellar profiles were blended. Hence it is likely that flux from one object contaminates the other, and the extracted spectra are still composite to some extent. However, using the STARLINK package *figaro*, we were able to extract a spectrum for both the primary and secondary

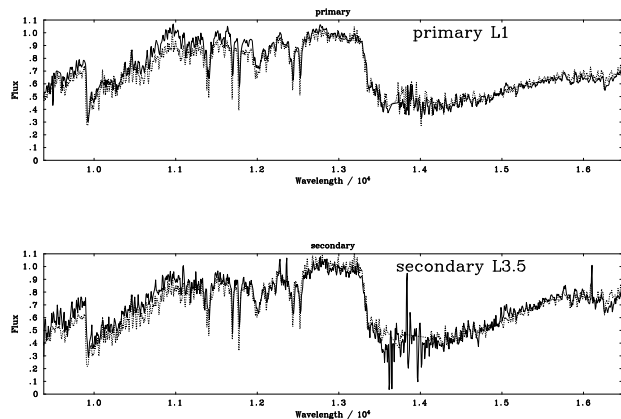


**Figure 10.** Spectral types for the two components by direct comparison to the Cushing et al. (2005) objects 2M1439+19 (L1) and 2M0036+18 (L3.5).

component separately. Fig. 10 shows the two separate spectra for which we estimate  $\sim L1$  and  $\sim L3.5$  for the primary and secondary components, respectively, by direct comparison to two Cushing et al. (2005) templates.

Furthermore, we employed the  $H_2OA$  and  $H_2OB$  indices of McLean et al. (2003) to estimate spectral types of L2.5 and L1.5 for the primary, and L4 and L4.5 for the secondary, consistent with the results shown in Fig. 10 to within  $\pm 1$  subclass. Hence the derivation of L4.5 for the composite spectrum (Fig. 6 and Table 2) seems strange. However, it is possible that a misalignment of the slit might have caused the earlier observation to be of the secondary alone, without much contribution from the primary.

We were unable to perform photometric measurements accurately on the acquisition image owing to a lack of calibration data. However, the strength of the stellar profiles in the two-dimensional spectra taken on 2006 April 11 are approximately in the ratio 1:2.5, i.e. the primary is 2.5 times brighter; one magnitude. Adopting spectral types L2 and L4 for the two components, we can derive  $M_J = 12.3$  and  $13.1$  from the spectral type vs. absolute  $J$  magnitude relation of Cruz et al. (2003). This difference of  $\sim 1 \text{ mag}$  is exactly what is observed, implying that the data are quite consistent with both components lying at the same distance, and being physically associated. Indeed, the flux ratio of 1:2.5 observed, together with the 2MASS  $J$  magnitude, allow us to derive  $J = 14.57$  for the secondary and  $J = 13.60$  for the primary, and distances of 19.7 and 18.2 pc respectively. These two values are consistent within the likely errors. Suitable data are not available for a common proper motion test; the object is too far south to be in the SDSS data, for example. We conclude that 2M1520–44 is very likely a binary, and note that the secondary has a strong likelihood of being substellar.

## 7 CONCLUSIONS

Using a combination of optical and near-infrared survey data from SuperCOSMOS and 2MASS, twenty-one hitherto undescribed sources are shown to be ultracool dwarfs

with spectral types in the range M7 to L5.5 using low resolution spectroscopy from NTT/SOFI. The sample objects have *JHK* magnitudes and colours comparable to known late M and L dwarfs and are bright enough to have optical detections in digitised plate data. They have proper motions typically a few  $\times 10^2$  mas yr<sup>-1</sup>. Spectroscopic distances are derived, typically within 30 pc, showing these objects to be important additions to our knowledge of low-mass, low-luminosity objects in the Solar neighbourhood.

Two objects in particular, 2M1750–00 and 2M2255–57, are of particular interest, with spectral types L5–L6 and spectroscopic distances near 10 pc. The latter has a high proper motion, 1.5'' yr<sup>-1</sup>. These two objects are likely brown dwarfs. In common with the rest of the sample, they are of great interest for further study using AO, HST, or methane imaging, to uncover lower-mass, later type companions. There is circumstantial evidence for the existence of such companions from the spectroscopic data presented here. Furthermore, these two objects in particular merit a parallax determination.

We have found a further object, 2M1520–44, to be a resolved L dwarf binary consisting of L2 and L4 components, lying  $\sim 19$  pc distant. Further study should reveal this source as a common proper motion pair. As such, it may prove a useful test-bed for evolutionary models of very low-mass stars and brown dwarfs.

## ACKNOWLEDGMENTS

TRK acknowledges financial support from PPARC. He would also like to thank the staff at ESO La Silla and especially Valentin D. Ivanov for his support of this project. This research has made use of data obtained from the SuperCOSMOS Science Archive, prepared and hosted by the Wide Field Astronomy Unit, Institute for Astronomy, University of Edinburgh, which is funded by the UK Particle Physics and Astronomy Research Council. This research has benefited from the M, L, and T dwarf compendium housed at DwarfArchives.org and maintained by Chris Gelino, Davy Kirkpatrick, and Adam Burgasser. This research has made use of the SIMBAD database, operated at CDS, Strasbourg, France.

## REFERENCES

- Baraffe I., Chabrier G., Barman T.S., et al. 2003, *A&A*, 402, 701
- Bouy H., Martín E.L., Brandner W. & Bouvier J., 2005, *Astron. Nacht.*, 326, 969
- Burgasser A.J., Kirkpatrick J.D., Burrows A., Liebert J., Reid I.N., Gizis J.E., McGovern M.R., Prato L. & McLean I.S., 2003, *ApJ*, 592, 1186
- Burgasser A.J., McElwain M.W., Kirkpatrick J.D., Cruz K.L., Tinney C.G. & Reid I.N., 2004a, *AJ*, 127, 2856
- Burgasser A.J., 2004b, *ApJ*, 614, L73
- Burgasser A.J. & Kirkpatrick J.D., 2006, *ApJ*, 645, 1485
- Chiu K., Fan X., Leggett S.K., Golimowski D.A., Zheng W., Geballe T.R., Schneider D.P. & Brinkmann J., 2006, *AJ*, 131, 2722
- Cruz K.L., Reid I.N., Liebert J., Kirkpatrick J.D. & Lowrance P.J., 2003, *AJ*, 126, 2421
- Cushing M.C., Rayner J.T. & Vacca W.D., 2005, *ApJ*, 623, 1115
- Deacon N.R., Hambly N.C. & Cooke J.A., 2005, *A&A*, 435, 363
- Epchtein N., 1997., in *The Impact of Large-Scale near-Infrared Surveys*, ed. F. Garzón, N. Epchtein, B. Burton & P. Persi (Dordrecht: Kluwer Academic Publishers), 15
- Hambly N.C., Irwin M.J. & MacGillivray H.T., 2001, *MNRAS*, 326, 1295
- Henry T.D., Lanna P.A., Kirkpatrick J.D. & Jahreiss H., 1997, *AJ*, 114, 388
- Henry T.D., Walkowicz L.M., Barto T.C. & Golimowski D.A., 2002, *AJ*, 123, 2002
- Henry T.D., Subasavage J.P., Brown M.A., Beaulieu T.D., Jao W.C. & Hambly N.C., 2004, *AJ*, 128, 2460
- Kirkpatrick J.D., Reid I.N., Liebert J., et al., 1999, *ApJ*, 519, 802
- Kirkpatrick J.D., Barman T.S., Burgasser A.J., McGovern M.R., McLean I.S., Tinney C.G. & Lowrance P.J., 2006, *ApJ*, 639, 1120
- Kendall T.R., Delfosse X., Martín E.L. & Forveille T., 2004, *A&A*, 416, L17
- Lawrence A., Warren S.J., Almaini O., Edge A.C., Hambly N.C., Jameson R.F., Lucas P., et al., 2006, *MNRAS*, submitted, astro-ph/0604426
- Leggett S.K., Allard F., Geballe T.R., et al., 2001, *ApJ*, 548, 908
- Lodieu N., Scholz R.-D., McCaughrean M.J., Ibata R., Irwin M. & Zinnecker H., 2005, *A&A*, 440, 1061
- Martín E.L., Delfosse X., Basri G., et al., 1999, *AJ*, 118, 2466
- McLean I.S., McGovern M.R., Burgasser A.J., Kirkpatrick J.D., Prato L. & Kim S.S., 2003, *ApJ*, 596, 561
- Phan-Bao N., & Bessell M.S., 2006, *A&A*, 446, 515
- Pokorny R.S., Jones H.R.A. & Hambly N.C., 2003, *A&A*, 397, 575
- Pokorny R.S., Dong C., Jones H.R.A. & Chapelle R.J., 2006, *A&A*, submitted
- Reid I.N., Burgasser A.J., Cruz K.L., Kirkpatrick J.D. & Gizis J.E., 2001, *AJ*, 121, 1710
- Reid I.N., Cruz K.L., Laurie S.P., et al., 2003, *AJ*, 125, 354
- Reid I.N., Lewitus E., Allen P.R., Cruz K.L. & Burgasser A.J., 2006a, *AJ*, 132, 891
- Reid I.N., Lewitus E., Burgasser A.J. & Cruz K.L., 2006b, *ApJ*, 639, 1114
- Scholz R.-D., Meusinger, H. & Jahreiss, H., 2005, *A&A*, 442, 211
- Skrutskie M.F., Schneider S.E., Steining R., et al., 1997, in *The Impact of Large-Scale near-Infrared Surveys*, ed. F. Garzón, N. Epchtein, B. Burton & P. Persi (Dordrecht: Kluwer Academic Publishers), 25
- Slesnick C.L., Hillenbrand L.A. & Carpenter J.M., 2004, *ApJ*, 610, 1045
- Subasavage J.P., Henry T.D., Hambly N.C., Brown M.A., Jao W.C. & Finch C.T., 2005, *AJ*, 130, 1658
- York D.G., Adelman J., Anderson J.E., et al., 2000, *AJ*, 120, 1579

**Table 1.** Basic data for the target objects. Optical magnitudes are taken from SuperCOSMOS and are on that photometric system; infrared magnitudes from the 2MASS All Sky Release, and are quoted on the 2MASS system. All the latter have photometric quality flags AAA ( $\text{SNR} \geq 10$  and  $\Delta JHK \leq 0.1$  mag.). Coordinates are taken from SuperCosmos at the given epoch. Proper motions and their errors are also derived from the SuperCOSMOS data and are given in units of  $\text{mas yr}^{-1}$ .

Name	2MASS	$\alpha$ (J2000)	$\delta$ (J2000)	$R$	$I$	$J$	$H$	$K$	epoch	$b$	$\mu_{\alpha \cos \delta}$	$\mu_{\delta}$	$\Delta \mu_{\alpha \cos \delta}$	$\Delta \mu_{\delta}$
M0004–20 <sup>4</sup>	00044144–2058298	00 04 41.20	–20 58 30.2	18.85	15.65	12.40	11.83	11.40	1995.362	–77.69	825.5	–9.2	75.7	75.5
M0005–21 <sup>1</sup>	00054844–2157196	00 05 48.21	–21 57 19.0	19.42	16.46	13.27	12.62	12.20	1995.244	–78.41	641.2	–159.2	89.4	88.3
M0123–42 <sup>2</sup>	01235905–4240073	01 23 59.14	–42 40 05.8	19.41	16.28	13.15	12.47	12.04	1994.038	–73.11	–140.5	–226.6	9.0	8.2
M0127–31 <sup>6</sup>	01273195–3140031	01 27 31.60	–31 40 05.1	18.75	15.79	12.66	12.04	11.66	1983.103	–80.93	324.3	108.5	27.0	25.3
M0128–55	01282664–5545343	01 28 26.86	–55 45 34.9	20.03	17.45	13.78	12.92	12.34	1992.197	–60.60	–248.8	153.9	19.1	19.0
M0228–63	02284355–6325052	02 28 42.52	–63 25 10.2	20.12	16.72	13.56	12.75	12.25	1989.630	–50.42	636.2	–25.1	261.3	247.1
M0352+02	03521086+0210479	03 52 10.63	+02 10 44.1	19.51	16.46	13.08	12.41	11.96	1988.990	–37.55	262.1	372.8	25.9	25.3
M0357–12	03574089–1249503	03 57 40.35	–12 50 02.3	19.27	15.67	13.46	12.84	12.44	1986.938	–44.26	132.7	–23.3	7.3	7.3
M0405–15	04054799–1515399	04 05 48.16	–15 15 24.8	21.28	18.95	13.55	12.93	12.52	1993.279	–43.47	–247.1	–133.5	27.7	26.7
M0511–46 <sup>3</sup>	05110163–4606015	05 11 01.59	–46 06 02.2	19.93	16.99	13.89	13.19	12.71	1994.452	–36.18	67.0	159.3	19.9	20.5
M0526–44	05264348–4455455	05 26 43.47	–44 55 44.7	20.00	17.53	14.08	13.31	12.71	1996.075	–33.34	13.4	–167.8	13.4	14.0
M0855–25	08555116–2512351	08 55 51.23	–25 12 32.7	19.59	16.44	13.25	12.62	12.20	1991.409	+12.81	–131.5	–363.7	22.0	21.3
M1019–27 <sup>5</sup>	10192447–2707171	10 19 24.80	–27 07 17.3	19.75	16.75	13.53	12.91	12.47	1992.168	+24.60	–643.2	36.6	21.6	20.2
M1146–39	11465791–3914144	11 46 58.18	–39 14 14.5	19.79	16.91	13.64	12.93	12.49	1989.332	+21.95	–292.4	4.3	11.7	10.5
M1347–76	13475911–7610054	13 47 57.97	–76 10 05.9	20.21	16.92	13.79	13.05	12.55	1980.818	–13.68	257.0	286.7	61.8	63.6
M1520–44	15200224–4422419	15 20 03.38	–44 22 34.8	19.42	16.89	13.23	12.36	11.89	1979.840	+10.84	–476.0	–566.7	84.4	85.0
M1523–23	15230657–2347526	15 23 06.58	–23 47 53.4	20.42	17.33	14.20	13.42	12.90	1989.427	+27.29	158.9	308.2	13.2	12.2
M1548–16	15485834–1636018	15 48 58.42	–16 36 00.8	19.93	17.04	13.89	13.10	12.64	1991.422	+28.64	–98.0	–161.2	43.3	41.5
M1750–00	17502484–0016151	17 50 25.16	–00 16 17.5	19.98	17.33	13.29	12.41	11.85	1986.661	+13.42	–440.4	217.5	43.3	41.1
M1842–39	18421930–3905574	18 42 19.48	–39 05 57.1	19.89	17.19	13.83	13.03	12.63	1980.664	–15.08	–621.4	–82.2	29.2	28.1
M1956–17	19561542–1754252	19 56 15.45	–17 54 25.3	20.09	16.88	13.75	13.11	12.65	1990.749	–22.12	–157.3	92.5	14.8	15.0
M2243–59	22431696–5932206	22 43 16.99	–59 32 18.4	20.24	17.37	14.07	13.39	12.84	1992.543	–50.85	–16.3	–243.1	23.8	23.4
M2255–57	22551861–5713056	22 55 18.74	–57 13 04.9	20.58	17.73	14.08	13.19	12.58	1995.217	–53.58	394.7	–1524.6	322.5	318.0
M2321–13	23211254–1326282	23 21 12.39	–13 26 27.1	20.73	17.77	14.50	13.58	13.14	1995.650	–64.88	550.0	–171.8	36.3	36.2

<sup>2,3</sup> Observed spectroscopically by Lodieu et al. (2005) with spectral types M8.5, L0.5 and M8.5 respectively

<sup>5</sup> Identified as high proper motion objects by Deacon et al. (2005)

<sup>6</sup> Identified as a high proper motion object by Pokorný et al. (2003)